



AC-DC FRONT END PFC FOR INDUCTION MOTOR DRIVE

¹B. Mosha Rani,²D.Ravi Kumar

¹M-tech Student Scholar, Department of Electrical & Electronics Engineering, Sri Mittapalli college of Engineering Tummalapalem, Guntur, Ap.

²Assistant Professor, Department of Electrical & Electronics Engineering, Sri Mittapalli college of Engineering Tummalapalem, Guntur, Ap.

ABSTRACT: Induction motor (IM) is now replacing all other machines from industry due to distinguish features. The IM structure is simple, self-starting capability low maintenance cost and is reliability of motor. The Induction Motor (IM) control in industrial drives is widely acknowledged for many applications, flexible control features by using pulse-width controlled VSI device. The widespread use of electronic devices from single-phase ac supplies necessitates the increasing use of power factor corrected (PFC) power supplies in many applications including electronic equipment, computer servers, and consumer products. PFC power supplies provide low total harmonic distortion (THD) in the current drawn from the line and this is an increasingly important requirement. This work describes an isolated power factor corrected power supply that utilizes the leakage inductance of the isolation transformer to provide boost inductor functionality. The bulk capacitor is in the isolated part of the power supply allowing for controlled startup without dedicated surge limiting components. A control method based on switch timing and input/output voltage measurements is developed to jointly achieve voltage regulation and input power factor control. The Active-PFC device acts as front-end of VSI fed induction motor for better speed control features by changing the PWM duty cycle. The critical evaluation of proposed method is verified under rated speed conditions by using Matlab/Simulink platform, results are presented.

Key words: Induction motor (IM), total harmonic distortion (THD), power factor corrected (PFC)

passive diode rectifier/LC filter input combination, the resulting converter would be very bulky and heavy due to the size of the low-frequency inductors and capacitors. The most common approach to PFC is to use two-stage power conversion schemes. These two-stage schemes use a front-end ac-dc converter stage to perform ac-dc conversion with PFC with the output of

the front-end converter fed to a back-end dc-dc converter stage that produces the desired isolated dc output voltage

[5]. Using two converter stages in this manner, however, increases the cost, size, and complexity of the overall ac-dc converter, and this has led to the emergence of single-stage power-factor-corrected converters.

I. INTRODUCTION

Power-electronic converters are becoming popular for various industrial drives applications. In recent years also high-power and medium-voltage drive applications have been installed. To overcome the limited semiconductor voltage and current ratings, some kind of series and/or parallel connection will be necessary. Due to their ability to synthesize waveforms with a better harmonic spectrum and attain higher voltages, multi-level inverters are receiving increasing attention in the past few years. The ac-dc power supplies with transformer isolation are typically implemented with some sort of input power factor correction (PFC) to comply with harmonic standards such as IEC 1000-3-2 [2]-[4]. Although it is possible to satisfy these standards by adding passive filter elements to the traditional

In order to reduce the cost, size, and complexity associated with two-stage ac–dc power conversion and PFC, researchers have tried to propose single-stage converters that integrate the functions of PFC and isolated dc–dc conversion in a single power converter. Several single-phase [6]–[12] and three-phase [5] converters have been proposed in the literature, with three-phase converters being preferred over single-phase converters for higher power applications. Previously proposed three-phase single-stage ac–dc converters, however, have at least one of the following drawbacks that have limited their widespread use.

- 1) They are implemented with three separate ac–dc single stage modules
- 2) The converter components are exposed to very high dc bus voltages so that switches and bulk capacitors with very high voltage ratings are required.
- 3) The input currents are distorted and contain a significant amount of low-frequency harmonics because the converter has difficulty performing PFC and dc–dc conversion simultaneously.
- 4) The converter must be controlled using very sophisticated techniques and/or nonstandard techniques [6]–[12]. This is particularly true for resonant-type converters that need variable-switching-frequency control methods to operate.
- 5) The output inductance must be very low, which makes the output current to be discontinuous. This results in a very high output ripple so that secondary diodes with high peak current ratings and large output capacitors to filter the ripple are needed.
- 6) Most of them are in discontinuous conduction mode at the input and need to have a large input filter to filter out large high-frequency harmonics [5].

2 Proposed Architecture

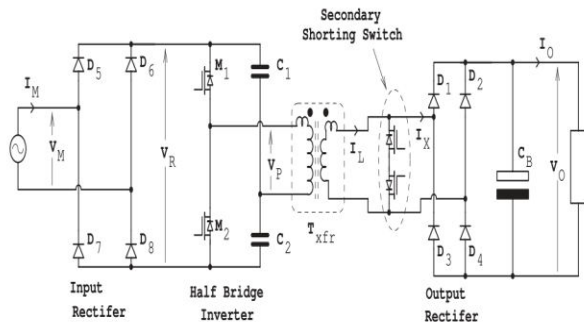


Fig. 1. Circuit diagram of the proposed power supply architecture.

The circuit diagram of the proposed power supply is shown in Fig. 1. A conventional four diode full wave rectifier rectifies the input ac source voltage producing a voltage V_R . This voltage is inverted to the high frequency f_s with a half-bridge inverter before being applied to a high-frequency transformer Txfr. The half-bridge inverter consists of the two switches M1 and M2 operated out of phase with a 50% duty cycle at the switching frequency f_s and the capacitive divider formed by C1 and C2.

The capacitors C1 and C2 prevent dc current flowing through the transformer primary and causing saturation problems. The values of C1 and C2 are chosen sufficiently small, such that at the mains frequency f_{AC} and low power level, they allow the rectifier output voltage V_R to follow the input mains waveform envelope. However, at the switching frequency, their values are sufficiently large to act as fixed voltage sources and not resonate with the transformer inductances or load. For the circuit of Fig. 1. The mains input voltage is $V_M(t) = \sqrt{2}V_{AC} \sin(2\pi f_{AC}t)$, with V_{AC} being the rms input voltage and $V_R(t)$ being the input voltage fully rectified. The transformer primary voltage $V_P(t)$ switches at the high frequency rate f_s , but with an amplitude of half $V_R(t)$, due to the half-bridge configuration.

The symbol for the transformer in Fig. 1 is drawn to emphasize that the transformer leakage inductance is used in the circuit rather than the usual case whereby leakage inductance is minimized as much as possible. The key to the operation of the circuit is the bidirectional secondary shorting switch shown in Fig. 1 [21].

3 THEORY OF OPERATION

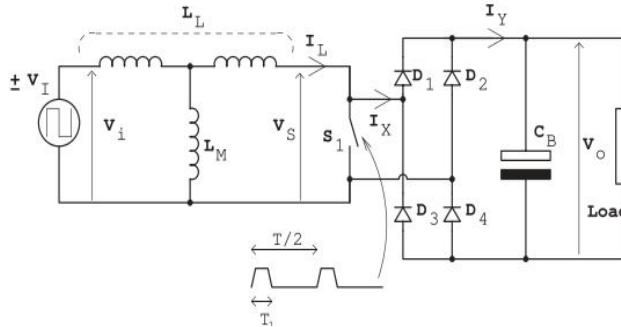


Fig. 2. Simplified circuit model for the proposed power supply.

Fig. 2 shows a simplified circuit model for the proposed power supply. Assuming the switching frequency of the converter is very high compared to the ac source frequency, the input to the transformer can be considered to be essentially a 50% duty cycle square wave with period T and peak amplitude $\pm V_I$. The model in Fig. 2 is referenced to the secondary side of the transformer and the voltage amplitude into the transformer model is the primary voltage $V_P(t)$ multiplied by the turns ratio of the transformer, or at time $t = kT$.

$$V_I[kT] = \left| V_P(kT) \frac{N_s}{N_p} \right| \quad (1)$$

The operation of the circuit is based on the assumption that the transformer magnetizing inductance L_M has little effect on the operation of the circuit other than to add a magnetizing current to the input source. Simulations show that magnetizing currents significantly less (a factor of $1.5 \times$ or less), than the currents being transferred, have little impact on the circuit overall functionality. The total leakage inductance of the transformer is denoted as L_L and the current flowing out of the transformer secondary winding is denoted as $I_L(t)$.

The operation of the system is essentially that of a step up or boost converter and is based around the timing of shorting switch S_1 in Fig. 2. At the beginning of a switching cycle, the input voltage switches to $+V_I$ (dropping the $[kT]$ for notation for

clarity) and simultaneously the shorting switch S_1 is turned ON. The current $I_L(t)$ in the leakage inductance L_L rises linearly while the switch S_1 is ON. When the switch S_1 is turned OFF, the current in the leakage inductance is forced through the rectifier diode bridge formed by $D_1, D_2, D_3,$ and D_4 , and into the capacitor C_B and system load, and the current in the leakage inductance falls. After a period of T_2 , the input voltage changes sign to $-V_I$ and the same operation occurs, except for a change in the sign of the inductor current. Two distinct operation modes of the circuit can be identified depending on whether the leakage inductance current starts at zero and returns to zero before time T_2 , denoted as the discontinuous conduction mode (DCM), or when the leakage inductance current starts the cycle with a nonzero (negative) value, retains a nonzero (positive) value at time T_2 and returns to a nonzero (negative) value at the end of the cycle (time T), denoted as the continuous conduction mode (CCM).

To achieve unity power factor, the circuit needs to be operated in such a manner as to control the input current drawn from the supply. The two operating modes are now discussed in detail to relate the input current drawn to the timing period T_1 .

3.1 Discontinuous Conduction Mode

Fig. 3(a) shows the input voltage $V_i(t)$, the secondary voltage $V_S(t)$, the leakage inductor current $I_L(t)$, and the current into and out of the output rectifier $I_X(t)$ and $I_Y(t)$ as well as the switch current $I_{S1}(t)$, for the circuit operating in DCM. With the shorting switch S_1 closed, the leakage inductor current $I_L(t)$ rises from zero to the value $+I_P$ over the set period T_1 , thus

$$I_P = V_I T_1 / L_L \quad (2)$$

When the shorting switch S_1 opens, the inductor current falls back to zero over a period T_2 with the relationship

$$I_P = (V_O - V_I) T_2 / L_L \quad (3)$$

The sum of the periods must be less than the half period $T/2$ to ensure operation in the DCM or

$$T_1 + T_2 \leq \frac{T}{2} \tag{4}$$

The average input current to the transformer model (ignoring the magnetizing inductance) over the period $T/2$ can then be calculated as follows:

$$I_L^* = \frac{1}{2} I_P \frac{T_1 + T_2}{\frac{T}{2}} \tag{5}$$

And combining with (2) and (3), the average input current is

$$I_L^* = \frac{T_1^2}{TL_L} \left(\frac{V_I V_O}{V_O - V_I} \right) \tag{6}$$

The actual input current from the ac source is a scaled version of this current and is

$$I_M = \frac{1}{2} \frac{N_s}{N_p} I_L^* \tag{7}$$

With any contribution from the magnetizing inductance averaging to zero over each T period.

It is apparent by considering (1) and (7), that achieving unity power factor in the input source is equivalent to controlling the current value $I^* L$ to be directly proportional to V_I . Denoting the constant of proportionality as GM , or $I_L^* = GM V_I$, then substituting in (6) and rearranging yields the equation

$$T_1 = \sqrt{GM T L_L \left(\frac{V_O - V_I}{V_O} \right)} \tag{8}$$

The equation shows that given a constant of proportionality as GM , the required time period T_1 can be calculated by knowledge of the system parameters L_L and T , measurement of the output voltage V_O and calculating V_I by measurement of the rectified input source voltage and scaling by a factor of $1/2$ NN sp

3.2 Continuous Conduction Mode

Fig. 3(b) shows the input voltage $V_i(t)$, the secondary voltage $V_s(t)$, the leakage inductor current $I_L(t)$, and the current into and out of the output rectifier $I_X(t)$ and $I_Y(t)$ as well as the switch current $I_{S1}(t)$, for the circuit operating in CCM. With the shorting switch S_1 closed, the leakage inductor current $I_L(t)$ rises from the value $-I_E$ to the value $+I_P$ over the set period T_1 , thus

$$I_P + I_E = V_I T_1 / L_L \tag{9}$$

When the shorting switch S_1 opens, the inductor current falls back to $+I_E$ over a period $T_2 = T/2 - T_1$ with the relationship

$$I_P - I_E = (V_O - V_I) T_2 / L_L \tag{10}$$

The average input current to the transformer model (ignoring the magnetizing inductance) over the period $T/2$ can then be calculated as follows:

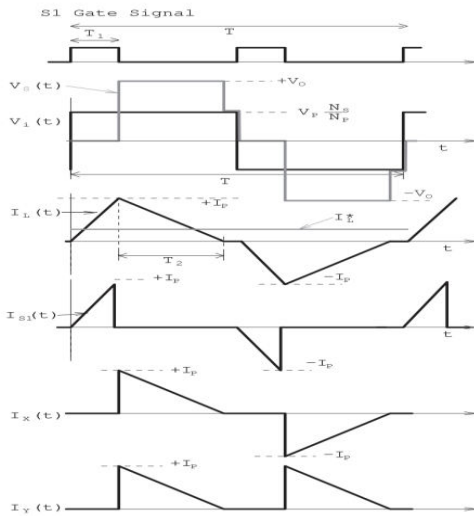
$$I_L^* = \frac{\frac{1}{2}(I_P - I_E)T_1 + \frac{1}{2}(I_P + I_E)T_2}{\frac{T}{2}} \tag{11}$$

And combining with (9) and (10), the average input current can be shown as

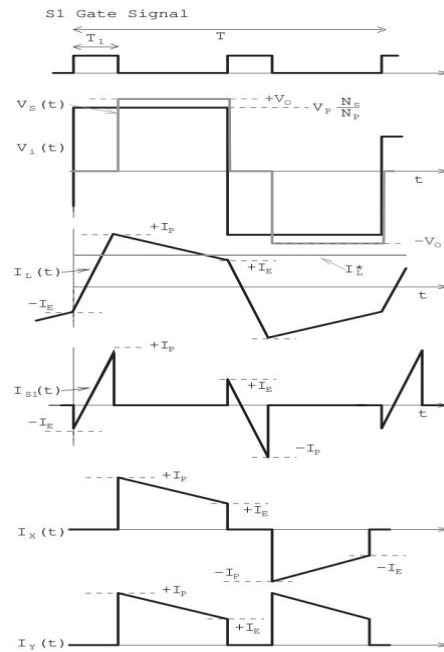
$$I_L^* = \left(T_1 \frac{T}{2} - T_1^2 \right) \frac{V_O}{T L L}. \tag{12}$$

With $I^*L = GM VI$, then substituting in (12) and rearranging yields the equation

$$T_1 = \frac{T}{4} \left(1 - \sqrt{1 - \frac{16G_M L L V_I}{T V_O}} \right). \tag{13}$$



(a) Discontinuous conduction mode.



(b) Continuous conduction mode.

Fig. 3 Idealized waveforms. (a) Discontinuous conduction mode. (b) Continuous conduction mode.

3.3 Power Handling Capability

The power capability of converter is determined by the maximum value of GM supported, which is limited by the requirement for (13) to result in a real number. This requires the argument under the square root to be non-negative, and hence

$$\frac{16G_{M \max} L L V_I}{T V_O} \leq 1$$

$$P_{\max} = \frac{1}{2} G_{M \max} V_{I \max}^2 \text{ of}$$

$$P_{\max} \leq \frac{V_{AC} \frac{N_s}{N_p} V_O}{32\sqrt{2} f_s L L}. \tag{14}$$

This equation can be used as a basis for converter design as demonstrated by the prototype example in

Section V. The maximum peak current in the leakage inductor during the CCM can be calculated as follows:

$$I_{P_{max}} = \frac{V_O T}{8L_L} \tag{15}$$

And the transformer must be designed to handle this peak current without saturation.

4. POWER SUPPLY CONTROL

The control objective for the power supply is to provide a constant output voltage and unity input power factor. This requires measurement of the output voltage and adjustment of the input current through the GM factor defined in Section III-A. However, calculating the time parameter T1 in Section III-A and III-B also requires knowledge of the parameter LL, the leakage

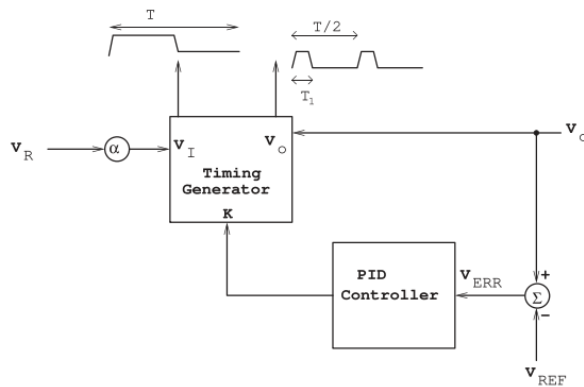


Fig. 4 Feedback control for the power supply.

Inductance, which may not be accurately known. Therefore a new control parameter K is defined as follows:

$$K = \frac{G_M L_L}{T} \tag{16}$$

And K is used for control rather than GM. Substituting into (8) and (13) results in the required calculations for DCM as

$$T_1 = T \sqrt{K \left(\frac{V_O - V_I}{V_O} \right)} \tag{17}$$

And CCM as

$$T_1 = \frac{T}{4} \left(1 - \sqrt{1 - \frac{16KV_I}{V_O}} \right). \tag{18}$$

It can further be shown that the boundary condition of (4) can be written as follows:

$$V_O(1 - 4K) \geq V_I. \tag{19}$$

The feedback loop of Fig. 4 can then be used to control the power supply. In Fig. 4, the power supply output voltage VO is measured and compared to a reference voltage VREF to produce an output voltage error VERR = VO - VREF. This error voltage is used by a PID controller with dynamics below the input ac frequency fAC to adjust the variable K to control the output voltage VO.

The variable K, is used in the timing generator to generate the inverter timing and the secondary shorting period T1 twice per sample period T. The timing generator uses the measured power supply output voltage VO, and a scaled version of the input rectifier voltage VR as VI = 1/2 NN sp VR. Using K, VI, and VO, the timing generator evaluates the condition in (19) and if the result is true, the DCM is selected and (17) is used to calculate the time period T1. Otherwise, the CCM is selected and (18) is used to calculate the time period T1.

III. INDUCTION MOTOR

An asynchronous motor type of an induction motor is an AC electric motor in which the electric current in the rotor needed to produce torque is obtained by electromagnetic induction from the magnetic field of the stator winding. An induction



motor can therefore be made without electrical connections to the rotor as are found in universal, DC and synchronous motors. An asynchronous motor's rotor can be either wound type or squirrel-cage type.

Three-phase squirrel-cage asynchronous motors are widely used in industrial drives because they are rugged, reliable and economical. Single-phase induction motors are used extensively for smaller loads, such as household appliances like fans. Although traditionally used in fixed-speed service, induction motors are increasingly being used with variable-frequency drives (VFDs) in variable-speed service. VFDs offer especially important energy savings opportunities for existing and prospective induction motors in variable-torque centrifugal fan, pump and compressor load applications. Squirrel cage induction motors are very widely used in both fixed-speed and variable-frequency drive (VFD) applications. Variable voltage and variable frequency drives are also used in variable-speed service.

In both induction and synchronous motors, the AC power supplied to the motor's stator creates a magnetic field that rotates in time with the AC oscillations. Whereas a synchronous motor's rotor turns at the same rate as the stator field, an induction motor's rotor rotates at a slower speed than the stator field. The induction motor stator's magnetic field is therefore changing or rotating relative to the rotor. This induces an opposing current in the induction motor's rotor, in effect the motor's secondary winding, when the latter is short-circuited or closed through external impedance. The rotating magnetic flux induces currents in the windings of the rotor; in a manner similar to currents induced in a transformer's secondary winding(s). The currents in the rotor windings in turn create magnetic fields in the rotor that react against the stator field. Due to Lenz's Law, the direction of the magnetic field created will be such as to oppose the change in current through the rotor windings. The cause of induced current in the rotor windings is the rotating stator magnetic field, so to oppose the change in rotor-winding currents the rotor will start to rotate in the direction of the rotating stator magnetic field. The rotor accelerates until the magnitude of induced rotor current and torque balances the applied load. Since rotation at synchronous speed would result in no induced rotor current, an induction motor always operates slower than synchronous speed. The difference, or "slip," between actual and synchronous speed varies from about 0.5 to 5.0% for standard Design B torque curve

induction motors. The induction machine's essential character is that it is created solely by induction instead of being separately excited as in synchronous or DC machines or being self-magnetized as in permanent magnet motors.

For rotor currents to be induced the speed of the physical rotor must be lower than that of the stator's rotating magnetic field (n_s); otherwise the magnetic field would not be moving relative to the rotor conductors and no currents would be induced. As the speed of the rotor drops below synchronous speed, the rotation rate of the magnetic field in the rotor increases, inducing more current in the windings and creating more torque. The ratio between the rotation rate of the magnetic field induced in the rotor and the rotation rate of the stator's rotating field is called slip. Under load, the speed drops and the slip increases enough to create sufficient torque to turn the load. For this reason, induction motors are sometimes referred to as asynchronous motors. An induction motor can be used as an induction generator, or it can be unrolled to form a linear induction motor which can directly generate linear motion.

Synchronous Speed:

The rotational speed of the rotating magnetic field is called as synchronous speed.

$$N_s = \frac{120 \times f}{P} \quad (\text{RPM}) \tag{20}$$

Where, f = frequency of the supply
P = number of poles

Slip:

Rotor tries to catch up the synchronous speed of the stator field, and hence it rotates. But in practice, rotor never succeeds in catching up. If rotor catches up the stator speed, there won't be any relative speed between the stator flux and the rotor, hence no induced rotor current and no torque production to maintain the rotation. However, this won't stop the motor, the rotor will slow down due to lost of torque, and the torque will again be exerted due to relative speed. That is why the rotor rotates at speed which is always less the synchronous speed. The difference between the synchronous speed (N_s) and actual speed (N) of the rotor is called as slip.

$$\% \text{ slip } s = \frac{N_s - N}{N_s} \times 100 \tag{21}$$

(IV) SIMULATION RESULTS:

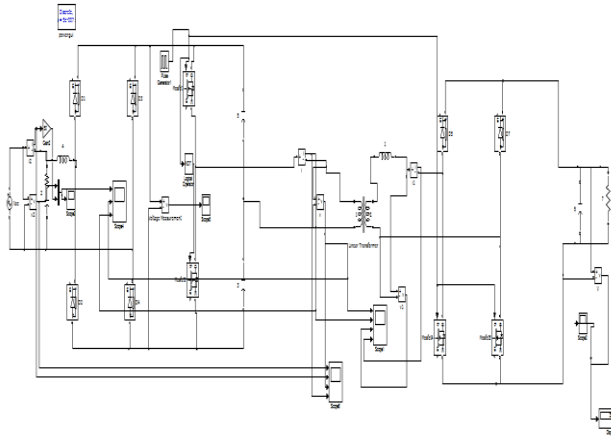


Fig 5 Simulink diagram of Proposed System Power Factor Corrected AC-DC power conversion

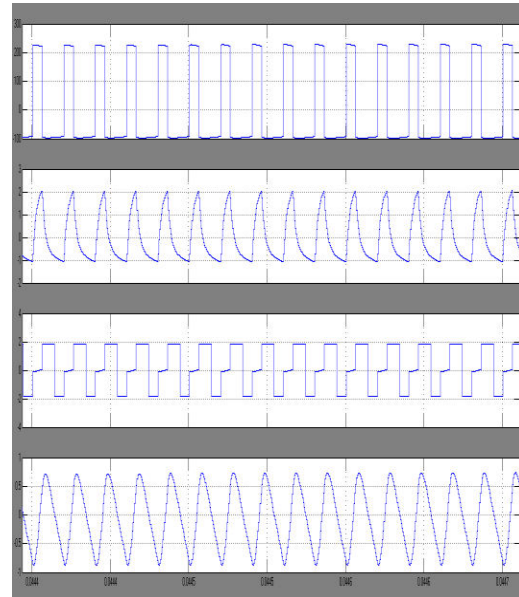


Fig. 6. Measured waveforms at 300 W operation, 1.5 ms from zero crossing and operating in DCM mode. Transformer primary voltage (VP) and current (IP) and secondary voltage (VS) and current (IS).

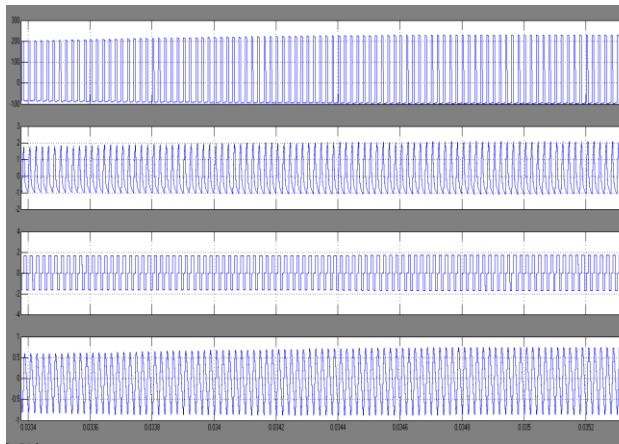


Fig. 6. Simulation waveforms at 300 W operation over a complete line cycle, input ac voltage (VAC) and current (IAC) and transformer primary voltage (VP) and current (IP)

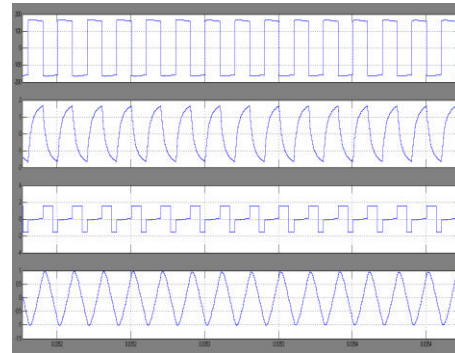


Fig. 7. Simulation waveforms at 300 W operation, 5 ms from zero crossing and operating in CCM mode. Transformer primary voltage (VP) and current (IP) and secondary voltage (VS) and current (IS).

Measured waveforms of the line input voltage and current and transformer primary voltage and current are shown in Fig. 5 over a full line cycle. Zoomed in waveforms of the transformer primary voltage and current and secondary voltage and current are shown in Fig. 6 (DCM) and Fig. 7 (CCM) and confirm the desired operation. The effect of finite values of bus capacitors C1 and C2 can be seen in the primary voltage waveform of Fig. 7 as a drop in the voltage rather than an ideal square wave.

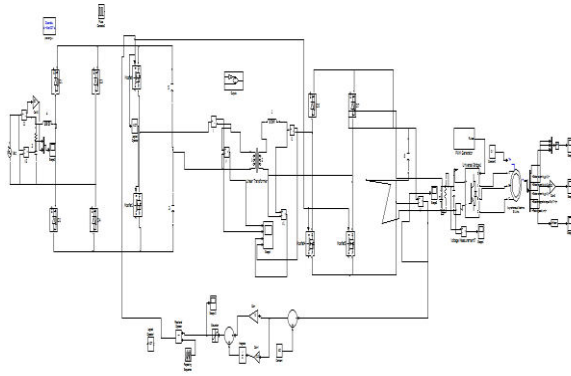


Fig 8 Simulink diagram of Proposed System Power Factor Corrected AC–DC power conversion with Induction Motor drive

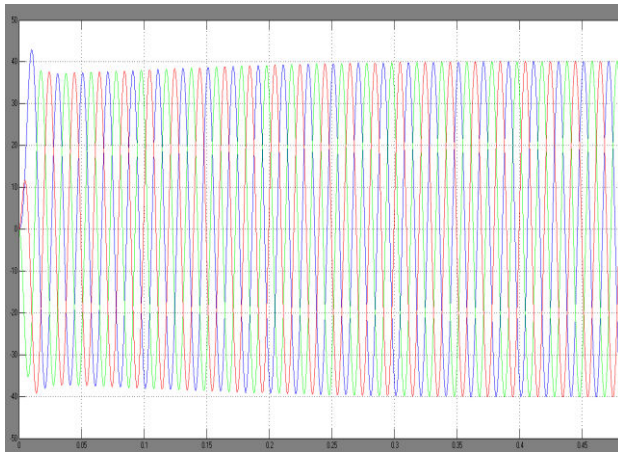


Fig 9 Simulation waveforms of Induction motor drive stator current characteristics

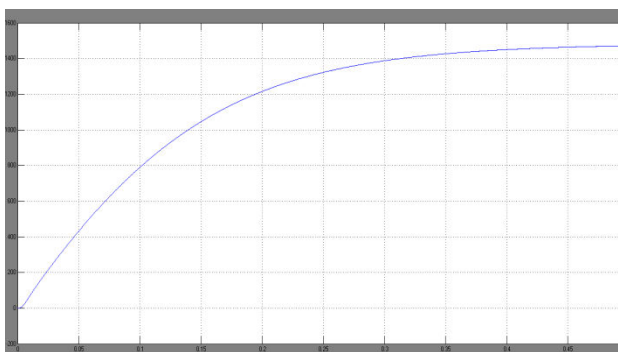


Fig 10 Simulation waveforms of Induction motor drive speed characteristics

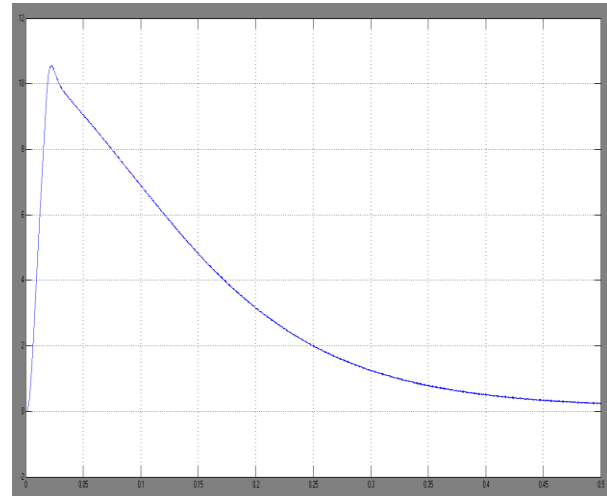


Fig 11 Simulation waveforms of Induction motor drive Torque characteristics

(V) CONCLUSION

This paper describes an isolated ac/dc power supply using the leakage inductance of the isolation transformer to achieve active power factor correction. The proposed with induction motor drive architecture allows for a compact lightweight power supply for power levels above that of fly back type PFC supplies. The principle of operation with two conduction modes is described and a timing based control method is developed for the power factor control. Measurements confirm the active power factor correction functionality with high power factor and low THD.

The proposed with induction motor drive power supply architecture is scalable and it should be feasible to extend the power capability of the proposed circuit to 500 W or more. Further variations on the principle can be adopted, such as universal input voltage operation, full bridge input inverter, zero current switching, synchronous rectification, interleaved designs, and so forth. The proposed architecture provides an additional option for the designers of PFC isolated supplies. And also verified the Induction motor characteristics.

REFERENCES

- [1] O. Garcia, J. A. Cobos, R. Prieto, P. Alou, and J. Uceda, "Single phase power factor correction: A survey," *IEEE Trans. Power Electron.*, vol. 18, no. 3, pp. 749–755, May 2003.
- [2] B. Singh, B. N. Singh, A. Chandra, K. Al-Haddad, A. Pandey, and D. P. Kothari, "A review of single-phase improved power quality AC-DC converters," *IEEE Trans. Ind. Electron.*, vol. 50, no. 5, pp. 962–981, Oct. 2003.
- [3] M. M. Jovanovic and Y. Jang, "State-of-the-art, single-phase, active powerfactor correction techniques for high-



- power applications—An overview,” *IEEE Trans. Ind. Electron.*, vol. 52, no. 3, pp. 701–708, Jun. 2005.
- [4] N. Mohan, T. M. Undeland, and W. P. Robbins, *Power Electronics: Converters, Applications, and Design*. Hoboken, NJ, USA: Wiley, Oct. 2002.
- [5] T. Yan, J. Xu, F. Zhang, J. Sha, and Z. Dong, “Variable-on-time-controlled critical-conduction-mode flyback PFC converter,” *IEEE Trans. Ind. Electron.*, vol. 61, no. 11, pp. 6091–6099, Nov. 2014.
- [6] D. G. Lamar, M. Arias, A. Rodriguez, A. Fernandez, M. M. Hernando, and J. Sebastian, “Design-oriented analysis and performance evaluation of a low-cost high-brightness LED driver based on flyback power factor corrector,” *IEEE Trans. Ind. Electron.*, vol. 60, no. 7, pp. 2614–2626, Jul. 2013.
- [7] C. Zhao, J. Zhang, and X. Wu, “An improved variable on-time control strategy for a CRM flyback PFC converter,” *IEEE Trans. Power Electron.*, vol. 32, no. 2, pp. 915–919, Feb. 2017.
- [8] J. W. Shin, S. J. Choi, and B. H. Cho, “High-efficiency bridgeless flyback rectifier with bidirectional switch and dual output windings,” *IEEE Trans. Power Electron.*, vol. 29, no. 9, pp. 4752–4762, Sep. 2014.
- [9] C.-P. Tung and H. S.-H. Chung, “A flyback AC/DC converter using power semiconductor filter for input power factor correction,” in *Proc. IEEE Appl. Power Electron. Conf. Expo.*, Long Beach, CA, USA, 2016, pp. 1807–1814.
- [10] L. Gu, W. Liang, M. Praglin, S. Chakraborty, and J. M. Rivas Davila, “A wide-input-range high-efficiency step-down power factor correction converter using variable frequency multiplier technique,” *IEEE Trans. Power Electron.*, vol. 33, no. 11, pp. 9399–9411, Nov. 2018.
- [11] K. Mino et al., “Novel bridgeless PFC converters with low inrush current stress and high efficiency,” in *Proc. Int. Power Electron. Conf.—ECCE ASIA*, Sapporo, Japan, 2010, pp. 1733–1739.
- [12] M. Alam, W. Eberle, and N. Dohmeier, “An inrush limited, surge tolerant hybrid resonant bridgeless PWM AC-DC PFC converter,” in *Proc. IEEE Energy Convers. Congr. Expo.*, Pittsburgh, PA, USA, 2014, pp. 5647–5651.
- [13] A. H. Memon, K. Yao, Q. Chen, J. Guo, and W. Hu, “Variable-on-time control to achieve high input power factor for a CRM-integrated buckflyback PFC converter,” *IEEE Trans. Power Electron.*, vol. 32, no. 7, pp. 5312–5322, Jul. 2017.
- [14] H. S. Athab, D. Dah-Chuan Lu, A. Yazdani, and B. Wu, “An efficient single-switch quasi-active PFC converter with continuous input current and low DC-bus voltage stress,” *IEEE Trans. Ind. Electron.*, vol. 61, no. 4, pp. 1735–1749, Apr. 2014.
- [15] S. W. Lee and H. L. Do, “A single-switch AC-DC LED driver based on a boost-flyback PFC converter with lossless snubber,” *IEEE Trans. Power Electron.*, vol. 32, no. 2, pp. 1375–1384, Feb. 2017.
- [16] J. I. Baek, J. K. Kim, J. B. Lee, H. S. Youn, and G. W. Moon, “A boost PFC stage utilized as half-bridge converter for high-efficiency DC-DC stage in power supply unit,” *IEEE Trans. Power Electron.*, vol. 32, no. 10, pp. 7449–7457, Oct. 2017.
- [17] M. A. Bakar and K. Bertilsson, “An improved modelling and construction of power transformer for controlled leakage inductance,” in *Proc. IEEE 16th Int. Conf. Environ. Elect. Eng.*, Florence, Italy, 2016, pp. 1–5.
- [18] R. Mitova, R. Ghosh, U. Mhaskar, D. Klikic, M. X. Wang, and A. Dentella, “Investigations of 600-V GaN HEMT and GaN diode for power converter applications,” *IEEE Trans. Power Electron.*, vol. 29, no. 5, pp. 2441–2452, May 2014.
- [19] A. M. Abou-Alfotouh, A. V. Radun, H. R. Chang, and C. Winterhalter, “A 1-MHz hard-switched silicon carbide DC/DC converter,” *IEEE Trans. Power Electron.*, vol. 21, no. 4, pp. 880–889, Jul. 2006.
- [20] J. S. Glaser et al., “Direct comparison of silicon and silicon carbide power transistors in high-frequency hard-switched applications,” in *Proc. 26th Annu. IEEE Appl. Power Electron. Conf. Expo.*, Fort Worth, TX, USA, 2011, pp. 1049–1056.
- [21] H. Wu, Y. Lu, T. Mu, and Y. Xing, “A family of soft-switching DC-DC converters based on a phase-shift-controlled active boost rectifier,” *IEEE Trans. Power Electron.*, vol. 30, no. 2, pp. 657–667, Feb. 2015.
- [22] C. A. Quinn and D. B. Dalal, “Empowering the electronics industry: A power technology roadmap,” *CPSS Trans. Power Electron. Appl.*, vol. 2, no. 4, pp. 306–319, Dec. 2017.